Journal of Colloid and Interface Science 674 (2024) 128–138

Contents lists available at ScienceDirect

Journal of Colloid And Interface Science

journal homepage: www.elsevier.com/locate/jcis

Ab initio modeling and experimental analysis of electronic conductivity in PEDOT:PSS-PEO films for extrusion-based manufacturing

Vitaliy Yurkiv [a,*], Xinnian Wang [b], Yongil Kim [b], Yayue Pan [b], Farzad Mashayek [a], Alexander L. Yarin [b,c]

[a] Department of Aerospace and Mechanical Engineering, University of Arizona, Tucson, AZ 85721, USA
[b] Department of Mechanical and Industrial Engineering, University of Illinois at Chicago, Chicago, IL 60607, USA
[c] School of Mechanical Engineering, Korea University, Seoul, Republic of Korea

HIGHLIGHTS

- The research incorporates both ab initio modeling and experimental analysis to explore the electronic conductivity of conducting polymers.
- Our results reveal that the addition of PEO to the PEDOT:PSS polymer blend results in a significant alteration in the band gap.
- At a maximum PEO content of 52 wt-%, there is a substantial increase in the electrical conductivity.
- The study finds that the ratio of PEDOT to PSS plays a pivotal role in determining the composite material's band gap.

GRAPHICAL ABSTRACT

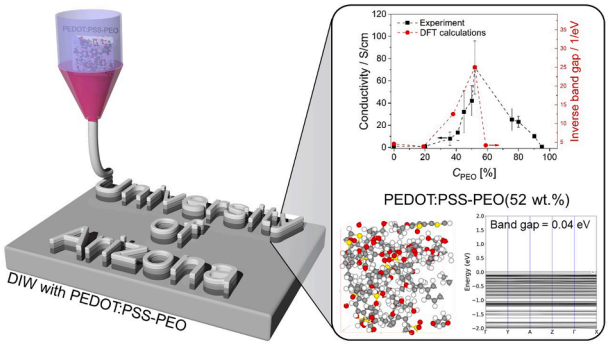

ARTICLE INFO

Keywords:
Density functional theory
Charge density
PEDOT:PSS

ABSTRACT

In this study, a combination of ab initio modeling and experimental analysis is presented to investigate and elucidate the electronic conductivity of films composed of conducting polymer blend PEDOT:PSS-PEO. Detailed density functional theory (DFT) calculations, aligned with experimental data, aided at profound understanding of the chemical composition, band structure, and the mechanical behavior of these composite materials. Systematic evaluation across diverse ratios of PEDOT, PSS, and PEO revealed a pronounced transformation in electronic properties. Specifically, the addition of PEO into the polymer matrix remarkably changes the band gap, with a marked alteration observed near a PEO concentration of 52 wt-%. This adjustment led to a substantial enhancement in the electrical conductivity, exhibiting an increase by a factor of approximately 20, compared to the original PEDOT:PSS polymer. The present investigation determined the crucial role of the PEDOT to PSS ratio in band gap determination, emphasizing its significant impact on the material's electrical conductivity. Concurrently, the mechanical property analysis unveiled a consistent increase in Young's modulus, reaching up to 765.93 MPa with increased PEO content, signifying a notable mechanical stiffening of the blend. The obtained combined theoretical and experimental insights illustrate a detailed perspective on the conductivity anomalies observed in PEDOT:PSS-PEO systems, establishing a robust framework for designing highly conducting and mechanically stable polymer blends. This comprehensive approach elucidates the interplay between chemical

* Corresponding author.
E-mail address: vyurkiv@arizona.edu (V. Yurkiv).

https://doi.org/10.1016/j.jcis.2024.06.148
Received 15 April 2024; Accepted 20 June 2024
Available online 22 June 2024

composition and electronic behavior, offering a strategic pathway for extrusion-based manufacturing techniques such as Direct Ink Writing (DIW).

1. Introduction

The ceaseless progress in organic-based technologies has spurred the advancement of electronic devices, including diodes, transistors, solar cells, and rechargeable batteries. A pressing need exists for conducting polymers that offer both high electrical conductivity and transparency, serving as essential charge transport layers and electrical interconnects in electronic devices. Blends of conducting polymers with high-molecular-weight non-conducting polymers have demonstrated remarkable viscoelastic properties, enabling direct ink writing (DIW) of conducting circuits on various materials, notably e-textiles, for diverse applications. Especially, the conducting polymer poly(3,4-ethylenedioxythiophene):poly(styrenesulfonic acid) (PEDOT:PSS) in combination with poly(ethylene oxide) (PEO) has emerged as a particularly promising candidate due to its exceptional film- and filament-forming characteristics, high transparency, tunable conductivity, and excellent thermal stability and processability [1]. The interest in such blends is driven by the efforts to improve the processability of PEDOT:PSS, especially, to tune properties such as viscosity and viscoelasticity, while minimizing the reduction in its electrical conductivity or even enhancing it [2–9]. Thus, in the present study, combining experimental and computational work, it is revealed how PEDOT to PSS to PEO ratio influences PDEOT:PSS-PEO electrical and mechanical properties, facilitating DIW for various applications.

It is apparent, based on the prior literature, that the interaction between PEO and PEDOT:PSS is complex, leading to unexpected properties. The ability of PEO to act as a secondary dopant hints at underlying mechanisms that may influence the composite's electronic and structural properties in ways that are beneficial for various applications. For Li-ion battery applications, a blend of PEDOT:PSS and PEO brings together the best of both polymers, offering a material that possesses both electronic and ionic conductivity, improved mechanical properties, and processability, as well as compatibility with different interfaces [10–12]. Yi et al. [3] and Wang et al. [4] reported that blending non-conducting PEO to PEDOT:PSS does not diminish the electrical conductivity but rather increases it. Yi et al. used a low-molecular-weight (M_w = 500 Da) PEO in blend with 5 % PEDOT:PSS solution in dimethyl sulfoxide (DMSO). As the content of PEO increased, the electrical conductivity exhibited an ascending trend, peaking at a PEO volume ratio of 0.5 %, after which it descended as the PEO volume ratio further increased. However, it should be emphasized that the processability of DMSO-based blends is low because of a very high boiling point of DMSO (189 °C) and, thus, very slow evaporation in an open atmosphere, and, accordingly, insufficiently slow precipitation and solidification of deposited polymeric material. Wang et al. [4] explored the effect of a relatively high-molecular-weight PEO ($M_w = 10^5$ Da) on aqueous suspensions of PEDOT:PSS. They found that the maximal electrical conductivity of 4.33 wt% aqueous suspension of PEDOT:PSS is reached at 52 wt% of PEO (in solidified PEDOT:PSS-PEO blend), with the enhancement in the conductivity by a factor of ~20 relative to that of the pure PEDOT:PSS.

Note that the PEO concentration corresponding to the peak electrical conductivity of PEDOT:PSS-PEO blends could be significantly affected by its molecular weight. For example, Kubarkov et al. [7] dispersed various weight ratios of dry PEDOT:PSS within a 2 wt% aqueous solution of high-molecular-weight PEO ($M_w = 1.0 \times 10^6$ Da) and found the peak electrical conductivity of deposited films at the 30 wt% PEO weight ratio. On the contrary, Fu et al. [13] reported that in their experiments, the electrical conductivity of PEDOT:PSS-PEO films gradually reduced with the addition of PEO. This outcome could potentially be attributed to a very high molecular weight PEO used ($M_w = 7 \times 10^6$ Da).

Lee et al. [6] explored the advancements in the fabrication and enhancement of PEDOT:PSS, a pivotal electrically-conducting polymer, with a focus on optimizing its conductive, stretchable, and transparent properties. They presented a comprehensive methodology that incorporates innovative treatments and processing techniques, resulting in a significant improvement in the material's characteristics. The study adeptly combines experimental investigations with theoretical insights to elucidate the underlying mechanisms that contribute to the enhanced performance of PEDOT:PSS. By ascertaining the potential of this modified polymer, Lee et al. underscore its relevance for next-generation electronic and optoelectronic applications.

Shahrim et al. [8] investigated the morphological and electronic transformations of PEDOT:PSS that develop upon doping, drawing attention to significant enhancements in electronic properties. Through a combination of experimental results and theoretical analyses, they elucidated the synergistic effects of dopant introduction and the consequential restructuring of the polymer matrix. Their comprehensive study offers a deeper understanding of the doping process, paving the way for the optimization of PEDOT:PSS-based devices in future research and applications.

Experimental measurements face challenges in understanding the electronic conductivity of polymers and their blends due to their complex structures, inherent inconsistencies from sample processing, and the limits of resolution in capturing detailed mechanisms. Density Functional Theory (DFT) offers a solution by providing detailed insights at the atomic and molecular levels, predicting material properties, and allowing studies under controlled conditions to isolate specific phenomena. There are several works focusing on evaluating the electronic properties of PEDOT:PSS and their blends based on experimental measurements [14–21]. One of the first reports on using the DFT to predict electronic properties of PEDOT:PSS was by Kim et al. [14] They comprehensively studied by DFT the doping processes of PEDOT, shedding light on the underlying electronic transitions. Through a series of simulations, they elucidated the response of the charge carriers in the polymer to the applied voltage, highlighting the mechanism of conductivity. The electronic structure and charge distribution of PEDOT were further explored using X-ray absorption spectroscopy and X-ray photoelectron spectroscopy. The findings from this investigation contribute to the understanding of PEDOT's electronic properties, offering insights beneficial for its application in electronic and optoelectronic devices.

Despite significant experimental and computational efforts toward the structure–property relationships of PEDOT:PSS-PEO blends, there remains a lack of studies that directly integrate experimental measurements of electronic properties with DFT calculations to delve into the exceptional electronic properties of these blends. In this study, a comprehensive investigation of the electronic conductivity of films composed of PEDOT:PSS-PEO is undertaken through a combined approach of ab initio modeling and experimental analysis. The DFT calculations have been performed based on experimental data to elucidate the chemical composition, the band structure, and the density of states of the composite materials. Incorporating DFT calculations alongside experimental measurements of the electrical conductivity offers a holistic approach to studying the electronic properties of PEDOT:PSS-PEO. The complementary nature of these methods provides a deeper, multifaceted understanding of the PEDOT:PSS-PEO properties, which holds great promise for future applications of highly conducting PEDOT:PSS-PEO blends.

2. Methodology

2.1. Experimental section

Material preparation. An aqueous suspension of Poly (3,4-ethylenedioxythiophene) polystyrene sulfonate (PEDOT:PSS) with a concentration of approximately 1 wt% (CLEVIOS™ PH 1000) was obtained from Heraeus, Germany. Additionally, polyethylene oxide (PEO, $M_v = 10^5$ Da) was procured from Sigma-Aldrich, USA. Both materials were used without further modification. The PEDOT:PSS suspension was subsequently blended with PEO powder in several weight percentages, specifically: γ = 20, 36, 40, 45, 50, 52, 75.8, 80, and 90.2 wt%. It is pivotal to highlight that γ represents the proportion of the PEO solid mass (M_{PEO}) relative to the cumulative solid mass (M_t), i.e., $\gamma = M_{PEO}/M_t$. To ensure homogeneity and stability of the resulting suspensions of such blends, they underwent magnetic stirring for a duration of 17 h under ambient conditions.

Measurement of the electrical conductivity. The aqueous PEDOT:PSS-PEO blends at any specific PEO concentration were printed onto a glass slide (EISCO, USA) using the DIW technique, which formed 2 cm × 2 cm thin square films. Subsequently, the printed films were dried in air at 60 °C for 30 min to evaporate water, precipitate the polymers and obtain solid films. Then, their thickness t was measured using a profilometer (SERIES 543, Mitutoyo, Japan). The four-point probe method was employed to measure the electrical conductivity S of the printed films. A source meter (Keithley 2400, Keithley, China) supplied the electric current I to the outer two probes, whereas a multimeter (Fluke 8845A, Fluke Co., USA) measured the potential ΔV between the inner two probes. Then, the sheet resistances R_s and the electrical conductivity S were calculated as:

$$R_s = \frac{\pi}{\ln(2)}\frac{\Delta V}{I}, \quad S = \frac{1}{R_s h} \tag{1}$$

where h is the measured film thickness (~0.2 mm).

Each conducting ink was used to print six different specimens, and each of them was evaluated twice at the same location on the film. In other words, 12 measurements were conducted for each case, and the average electrical conductivity value and deviation were reported.

Measurement of PEDOT:PSS-PEO density. First, the weight of the clean glass slide M_g was measured. Subsequently, a thin film was meticulously fabricated on each glass slide, as described above (cf. *Material preparation*). Then, the total weight of the specimen M_s, including both the solid film and the glass slide, was measured. The mass of the solid film $M = M_s - M_g$ was determined (~0.16 g), and the volume of the solid film was found as a product of the measured width (w), length (l), and thickness h of the specimen $V = w \times l \times h$ (~20 mm × 20 mm × 0.2 mm = 80 mm^3), Accordingly, the density of PEDOT:PSS-52 wt% solid specimens was found as $\rho = M/V$.

Measurement of crystallinity. The degree of crystallinity in PEDOT:PSS-52 wt% PEO thin films was measured using an X-ray diffraction (XRD) analyzer (Bruker D8 Discovery, Bruker, USA). During the scanning process, the specimens were scanned from 0° to 70° at the rate of 0.01°/s at room temperature. Then, the degree of crystallinity χ_c was calculated as [22]

$$\chi_c = \frac{A_c}{A_c + A_a} \tag{2}$$

where A_c is the area of the crystalline peaks, and A_a is the area of the amorphous peaks.

Measurement of hydration. TA Instruments' Q5000 (USA) was used to perform thermogravimetric analysis (TGA) of dry PEDOT:PSS-52 wt% PEO. Nitrogen was used to purge all the operations. Temperature was increased from 25 to 200 °C at a rate of 5 °C/min during the heating process.

2.2. Computational section

In the present study, Quantum ATK was employed to generate atomic configurations of both crystalline and polymeric forms of PEDOT, PEDOT:PSS, and PEDOT:PSS-PEO composites. Then, DFT [22] calculations were conducted utilizing the Vienna Ab initio Simulation Package (VASP) [23–25] code. Below, the structural generation process using ATK is discussed first, followed by a description of the DFT computational approach in VASP.

ATK methodology. Crystalline PEDOT and PEDOT:PSS structures were created based on atomic configurations available in the literature [14,20,21]. Fig. S1a in Supplementary Material illustrates these structures, where the crystalline PEDOT is depicted on the left, while PSS-doped PEDOT is depicted on the right. To build the polymeric PEDOT:PSS-PEO with different PEO contents, Quantum ATK Polymer Builder was utilized using EDOT, SS and EO monomers, as shown in Fig. S1b. The Polymer Builder is adept at constructing both crystalline and amorphous polymer configurations, making it a versatile tool for various applications. The creation of the polymer structures begins with the definition of a repeat unit or a monomer (EDOT, SS and EO). These monomer units act as a foundational block for a subsequent polymer chain. Each monomer is then repeated in a specified manner to form polymer chains. The chain length, determined by the degree of polymerization, is adjustable, allowing for the generation of polymers of desired lengths. For amorphous polymers, the process involves the generation of random configurations. This was achieved by placing polymer chains in a simulation box, followed by the application of a melt-quench procedure. The melt-quench methodology entails heating the system to a temperature of 1000 K, which is above the used polymers melting point, to ensure sufficient chain mobility. Subsequently, the system is rapidly cooled or quenched to room temperature, around 300 K, within a nanoseconds time span using a quenching rate of 10^{10} K/s. This abrupt temperature transition results in a disordered, non-crystalline arrangement of the polymer chains, characteristic of amorphous polymers. Thus, the Polymer Builder tool in Quantum ATK offers a systematic and comprehensive approach for constructing both crystalline and amorphous polymer structures. By defining the monomer and adjusting such parameters as the degree of polymerization, lattice symmetry, and quenching rate, one can tailor the corresponding generated configurations to match specific requirements. Specifically, in the present case, PEDOT:PSS ratio was kept constant, while EO content was adjusted to obtain the desired PEDOT:PSS-PEO composition. This results in a well-mixed polymer chains as depicted in Fig. S2.

DFT methodology. In the presented research, the electronic structure calculations were performed utilizing the DFT as implemented in VASP. The exchange–correlation interactions were treated with the DFT-D2 method proposed by Grimme [26], which provides a semi-empirical correction for the van der Waals interactions, enhancing the accuracy of the DFT results for systems where dispersion forces play a significant role. A plane-wave basis set with a kinetic energy cut-off of 450 eV was employed for the electronic wave functions. For the structural optimizations, the convergence criteria were rigorously set. The optimizations were executed until the residual forces acting on all atoms were reduced to less than 0.01 eV/Å, ensuring the attainment of a true structural minimum. Furthermore, during the self-consistent field iterations, the convergence criterion for the change in total energy between successive electronic steps was stringently set to 0.1 meV. These stringent criteria ensure both the reliability and precision of the calculated results. VASP was employed to calculate both the electronic Density of States (DOS) and the band structure of materials. The DOS provides a measure of the number of electronic states available per energy interval, allowing for a detailed understanding of the electronic properties of a material. In VASP, the DOS is extracted from the electronic eigenvalues obtained in a self-consistent DFT calculation. Specifically, a self-consistent field (SCF) calculation is first performed to converge the electronic density. The DOS is then computed over a finer k-point mesh to obtain detailed

electronic state distributions as a function of energy. This is done using the DOSCAR file produced by VASP. The band structure provides a visualization of the energy of electronic states as a function of the wavevector, k. It offers insights into the electronic dispersion relations and the existence of any band gaps, crucial for semiconductors. To compute the band structure using VASP, first, an SCF calculation is performed to converge the charge density. Post convergence, a non-self-consistent field (NSCF) calculation is executed along specific high-symmetry k-path directions in the Brillouin zone to extract the electronic bands. The eigenvalues obtained from this calculation, are stored in the EIGENVAL file, are then processed to plot the band structure in ATK Builder. In the context of computing mechanical properties using VASP, a certain strain was applied to an optimized polymer blend; consequently, the response of a blend was evaluated in terms of changes in energy, allowing for the determination of elastic constants.

3. Results and discussion

In this section, we delve into the electronic conductivity properties of the PEDOT:PSS-PEO composite, integrating insights from both DFT simulations and measurements of the electrical conductivity. Through a combined approach of theoretical calculations and empirical data, a comprehensive understanding of the electric conductivity within the composite is aimed. The present study seeks to unravel the synergistic effects of PEDOT:PSS and PEO on the overall conductivity and to discern the interplay between the theoretical predictions and the experimental outcomes.

3.1. Experimental results

The electrical conductivity of PEDOT:PSS-PEO films. The average density of PEDOT:PSS-52 wt% PEO films was measured as 7.72 (±1.07) × 10^{-1} g/cm^3. The PEDOT:PSS-PEO electrical conductivity measurements were performed using a four-point probe method (cf. *Measurement of electrical conductivity*). The subsequent calculations using Eq. (1) yielded the sheet resistances and electrical conductivities of the films. Fig. 1 depicts a two-dimensional scatter plot with error bars, illustrating the relationship between C_{PEO} (percentage composition of PEO) on the horizontal axis and the electrical conductivity, S (in S/cm) on the vertical axis. The PEO percentage composition is in the 0–100 % range, indicating the PEO content in the sample. The vertical axis, labeled as S [S/cm], spans the 0 to 100 S/cm range, covering the conductivity values of the explored blends. The data points are plotted at various C_{PEO} percentages, each accompanied by numerical annotations indicating the exact conductivity value in S/cm. The error bars extend vertically from each data point, illustrating variability in the conductivity measurements at each given C_{PEO} percentage. The data exhibits a non-linear trend, beginning from the left, the conductivity values increase gradually from around 1.08 S/cm at 0 % PEO to a peak value of 72 S/cm at 52 % C_{PEO}. Beyond this point, the conductivity values decrease sharply, reaching a value of around 0.46 S/cm at 98 % C_{PEO}. The peak conductivity at 52 % C_{PEO} suggests an optimal PEO concentration in the PEDOT:PSS-PEO blend.

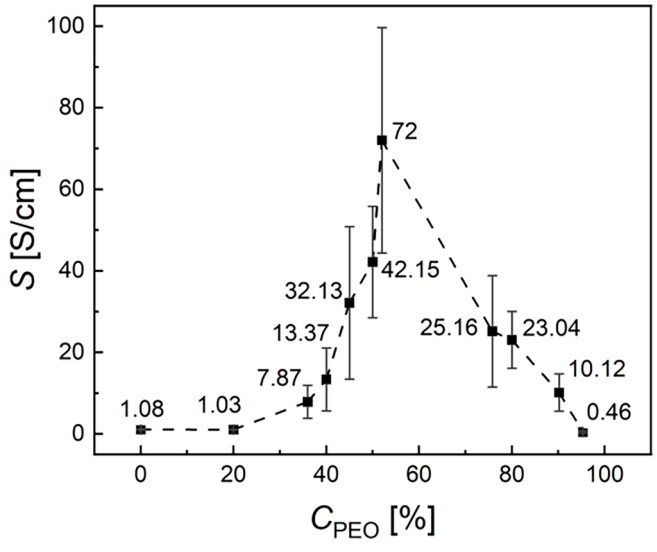

Fig. 1. Relationship between the concentration of C_{PEO} (%) and the electrical conductivity (S, S/cm). The data points represent the average conductivity values at each C_{PEO} concentration, with error bars indicating one standard deviation.

Crystallinity and hydration of PEDOT:PSS-PEO films. The XRD methods are powerful tools for measuring the crystallinity of materials. The intensity peaks in the XRD spectra typically represent the crystalline structure of the material [28]. The XRD analysis at room temperature as shown in Fig. 2a. Four major peaks were observed, which are related to semi-crystallinity of PEO. The low peaks at 2θ = 19.1°, 23.3°, 38.24°, and 44.51° correspond to (1 2 0), (0 3 2), (1 3 1), and (1 2 0) planes of PEO polymer, respectively. [27] A high bump over a wide range of 2θ represents an amorphous phase of the blends. [28] The degree of

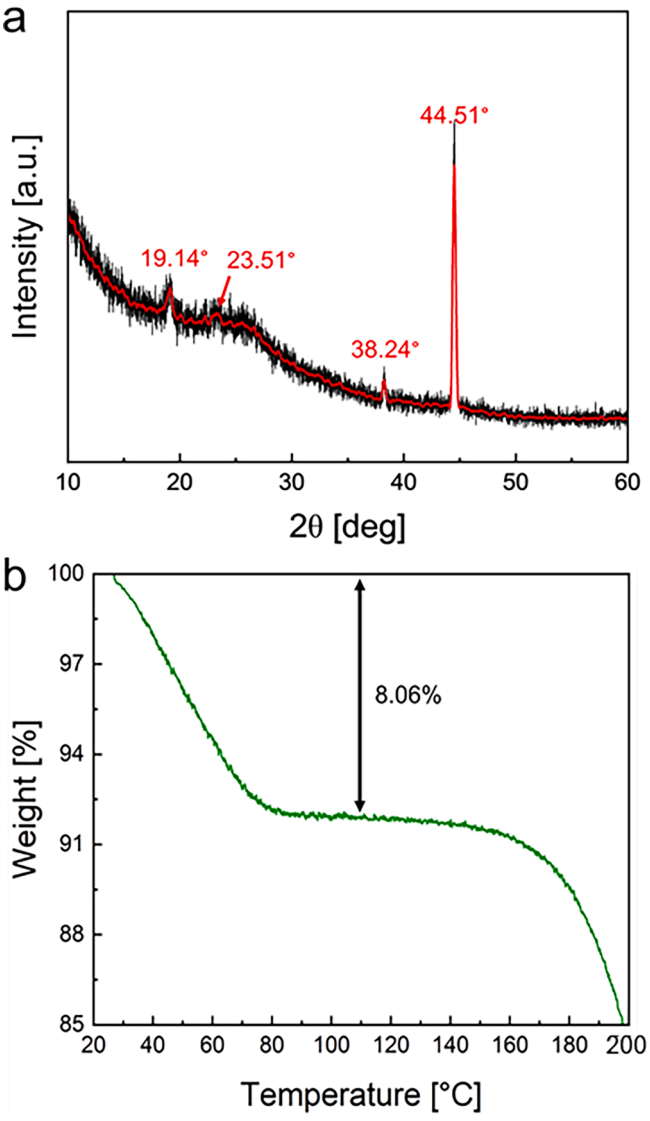

Fig. 2. (a) XRD results used to calculate the crystallinity of the PEDOT:PSS-52 wt% PEO film, (b) TGA results used to measure the hydration level of the PEDOT:PSS-52 wt% PEO.

crystallinity χ_c is evaluated as defined in Section 2.1 in Eq. (2). Based on Fig. 2a, the area of the crystalline peaks A_c was measured as 211.72, while the total area $A_c + A_a$ was measured as 8350.90. As a result, the degree of crystallinity for the dry PEDOT:PSS-52 wt% PEO composite was calculated as 2.54 %. The TA universal analysis by means of TGA was employed to analyze the degree of hydration of dry PEDOT:PSS-52 wt% PEO. Fig. 2b illustrates the weight reduction of the dry PEDOT:PSS-52 wt% PEO composite from room temperature to 200 °C, representing water removal of approximately 8.06 % (8 % at 92 °C).

3.2. *DFT results on the electronic structure of PEDOT, PEDOT:PSS, and PEDOT:PSS-PEO systems*

In this section, the electronic structure of crystalline and polymer variants of PEDOT, PEDOT:PSS, and PEDOT:PSS-PEO blends is calculated using the DFT calculations. First, the electronic characteristics of crystalline PEDOT and PEDOT:PSS are addressed. While comprehensive details pertaining to these materials are available in existing literature, the aim here is to recalculate the electronic structure, which stems from a desire to validate the present computational methodology and to ensure a robust alignment with previously reported results. Establishing this alignment instills confidence in the reliability and consistency of the present calculation approach and paves the way for further calculations aiming at polymeric PEDOT:PSS and PEDOT:PSS-PEO blends. As it is mentioned above, the experimental PEDOT:PSS-PEO polymers have an amorphous structure, that is why after establishing and validating our DFT calculation against crystalline literature available results, we proceed with calculations of amorphous structures. Thus, the DFT-derived band structures of the polymer form of PEDOT:PSS blended with PEO are discussed after the crystalline structure

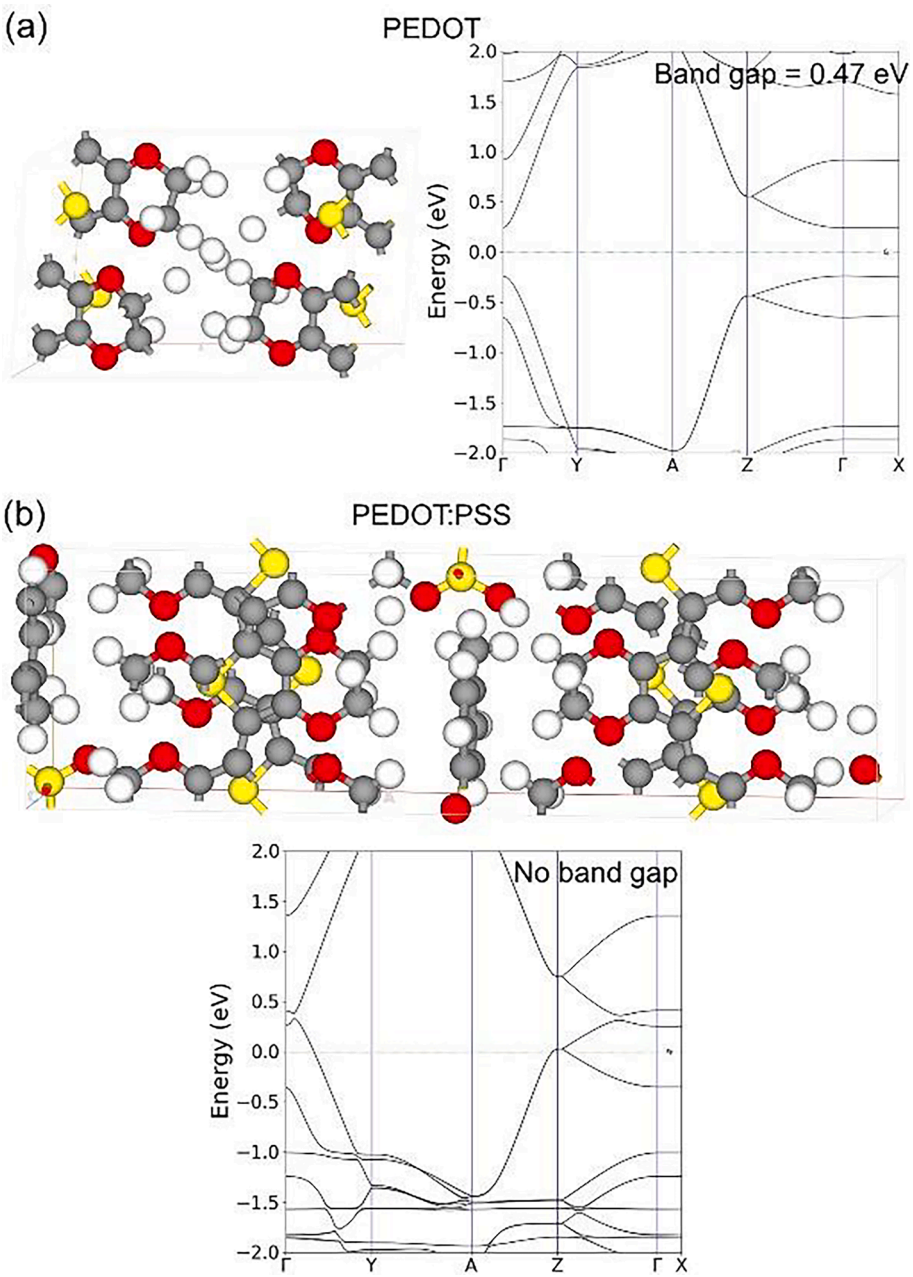

Fig. 3. Atomic structures and DFT-calculated band structures of crystalline (a) PEDOT and (b) PEDOT:PSS blend. Grey spheres depict carbon atoms, red spheres are oxygen atoms, yellow spheres are sulfur atoms, and white spheres denote hydrogen atoms. (For interpretation of the references to colour in this figure legend, the reader is referred to the web version of this article.)

calculations. Accordingly, the influence of varying PEO content on the electronic structure is carefully studied. Such an investigation is paramount to shedding light on how the incorporation of PEO alters the electronic properties of the blends, thereby offering insights into the potential benefits of PEO not only as a rheological modifier, but an electronic-performance enhancer in device applications. In the subsequent subsections, the computational details are outlined, the corresponding results are presented, and comparisons are drawn not only regarding successful comparisons with the established literature and our experimental results but also regarding the nuanced effects of PEO content on the electronic properties of PEDOT:PSS-PEO blends. At the end of the paper, the mechanical properties of blends and the discussion on the nature of electronic conductivity are presented.

3.2.1. Crystalline structures

Fig. 3 illustrates the atomic arrangement and the DFT-calculated band structures of crystalline PEDOT and PEDOT:PSS blend. The upper panel presents the atomic structure of crystalline PEDOT, delineating its distinct lattice arrangement. Adjacent to this depiction is the DFT-calculated band structure for the same material. The vertical axis in the right-hand side image represents the energy levels, measured in electron-volts (eV), spanning the −2.0 eV to 2.0 eV range. The horizontal axis displays the high-symmetry points in the Brillouin zone, labeled as Γ, Y, A, Z, Γ, and X. Several distinct electronic bands, represented by continuous curves, traverse this energy-k space. The bands depict the energy of the electronic states as a function of the wavevector, k, through the high-symmetry directions. The band structure reveals a conspicuous band gap of 0.47 eV, highlighting the semiconducting nature of crystalline PEDOT. This band gap represents the energy difference between the valence band (the highest occupied band) and the conduction band (the lowest unoccupied band). The Fermi level is indicated by a dashed horizontal green line that intersects the vertical axis at 0 eV. This line demarcates the energy level up to which the electronic states are occupied at absolute zero temperature. The inherent band gap corresponding to PEDOT suggests its potential as a semiconductor in electronic devices, especially in organic electronics and rechargeable batteries. However, the crystallinity in pure PEDOT might introduce challenges in terms of flexibility and processability, which are often sought after in wearable electronics and flexible displays. The reference to “pure” PEDOT serves as a simplified model to better understand the intrinsic properties of the PEDOT polymer, and is not meant to overlook the essential role of counterions (e.g., PSS) in real-world synthesis and applications of PEDOT.

The lower panel in Fig. 3 presents the atomic structure of the crystalline PEDOT:PSS blend, illustrating the integration of PSS within the PEDOT lattice. This is complemented by the corresponding DFT-calculated band structure. Contrasting with pure PEDOT (Fig. 3a), the PEDOT:PSS band structure does not manifest a band gap, alluding to its conductor-like behavior. The absence of a band gap in the PEDOT:PSS blend points to its potential use in applications that require conductive materials, such as electrodes in organic light-emitting diodes (OLEDs), or as transparent conductive films in touchscreens. The integration of PSS could improve the solubility and processability of PEDOT, making it more compatible with solution-based fabrication methods. Nonetheless, the blend’s conductor-like nature might compromise its use in applications where semiconducting behavior is essential, such as in field-effect transistors.

3.2.2. Polymer structures

Fig. 4 presents the DFT results for polymeric PEDOT structure. On the left, the intricate polymer structure of PEDOT is depicted, revealing its macromolecular arrangement. On the right, the DFT-calculated band structure for PEDOT is presented. The band structure distinctly demonstrates a band gap of 1.32 eV. Notably, this value aligns well with experimental data reported in the literature [1,29], reaffirming the computational precision. PEDOT’s observed band gap of 1.32 eV positions it as a potential candidate for various electronic applications. This energy range is particularly favorable for organic photovoltaics, where the alignment of the band gap with the solar spectrum can enhance light absorption and conversion efficiencies. Furthermore, the polymer nature of PEDOT often translates to inherent flexibility, making it a valuable material for emerging applications in flexible and wearable electronics. However, while the polymer structure offers advantages like flexibility and potential for solution-based processing, it might also present challenges. The macromolecular arrangement can sometimes lead to issues related to batch-to-batch variability, impacting the reproducibility of device performance. Additionally, the organic nature of PEDOT may pose concerns regarding long-term stability, especially when exposed to environmental factors such as moisture and oxygen.

In Figs. 3a and 4, the atomic and molecular configurations of crystalline and polymer PEDOT are illustrated, with their corresponding DFT-derived band structures elucidating the inherent electronic characteristics of each form. The difference in the band gap values, 0.47 eV for the crystalline form and 1.32 eV for the polymeric counterpart, indicates their distinct electronic behavior attributable to the inherent structural variations. The narrower band gap of crystalline PEDOT suggests its potential effectiveness in applications necessitating near-infrared absorption, encompassing specialized photodetectors or

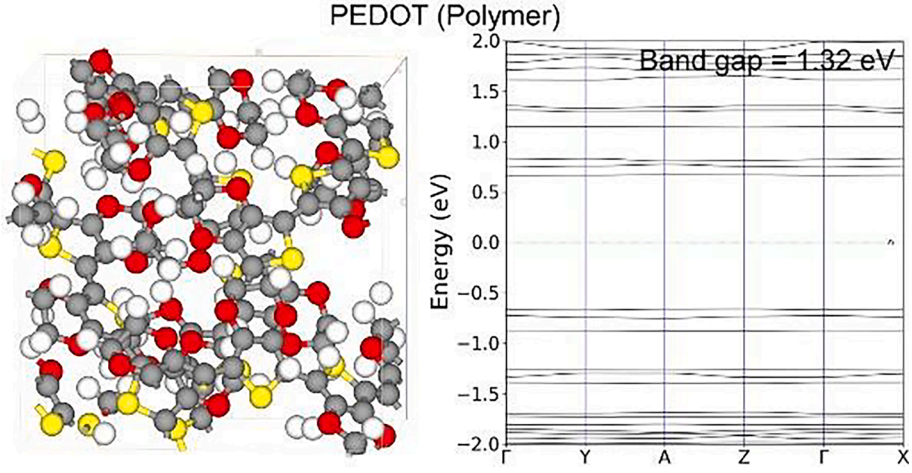

Fig. 4. Polymer structure (left) and DFT-calculated band structure (right) of PEDOT. A significant band gap of 1.32 eV is observed. Grey spheres depict carbon atoms, red spheres are oxygen atoms, yellow spheres are sulfur atoms, and white spheres denote hydrogen atoms. (For interpretation of the references to colour in this figure legend, the reader is referred to the web version of this article.)

specific photovoltaic configurations. Conversely, the pronounced band gap of the polymeric form of PEDOT aligns more favorably with the solar spectrum, emphasizing its prospective deployment in organic photovoltaic applications. Evidently, the observed disparities in the band structures can be traced back to the intrinsic differences in the atomic and molecular alignments between the two PEDOT conformations. The crystalline structure exhibits periodic and regimented atomic placements, revealing unique electronic band configurations. In association, the macromolecular structure of polymers can instigate a spectrum of electronic interactions, potentially ending in varied band gap magnitudes. It is imperative to highlight that the deduced band gap of 1.32 eV for polymer PEDOT exhibits commendable alignment with available experimental data. Such an agreement underscores the robustness of computational methodologies in predicting the electronic comportment of organic polymer substrates.

Fig. 5 demonstrates the atomic structures and the DFT-calculated band structures of polymer PEDOT:PSS in blends with varying PEO content. The figure unfolds over five vertically arranged panels, labeled from (a) to (e). Each panel is split, with the left segment portraying the atomic structure of polymer PEDOT:PSS, incorporating distinctive PEO content levels. The adjacent right segment of each panel depicts the corresponding DFT-calculated band structure, highlighting the consequential band gap alterations due to PEO integration. The PEDOT:PSS ratio of structures depicted in Fig. 5 corresponds to those experimentally studied in the present work 1:2.5 (cf. *Experimental results*).

In panel (a) in Fig. 5, the PEDOT:PSS structure devoid of PEO is presented, revealing a band gap of 0.22 eV. Progressing to panel (b), a 17 % PEO content in the polymer matrix leads to a slightly increased band gap value of 0.26 eV. However, as the PEO content increases to 38 % in panel (c), there is a marked reduction in the band gap to 0.08 eV. A further increment in the PEO content up to 52 % (cf. Fig. S2 for the atomic structure) corresponding to panel (d) results in a minimal band gap of 0.04 eV. Intriguingly, panel (e) exhibits an uptick in the band gap value to 0.25 eV, corresponding to a PEO content of 59 %. This systematic presentation highlights the particular relationship between the PEO content in blend with PEDOT:PSS and its impact on the electronic properties, as is evidenced by the varying band gaps. The 59 % PEO content is the largest PEO content possible in the present DFT calculations, because this atomic conformation consists of 502 atoms. The data presented in Fig. 5 underscores the capability to alter the electronic characteristics of PEDOT:PSS through strategic incorporation of PEO, potentially tailoring the material for specific optoelectronic applications. The modulation of the band gap in PEDOT:PSS as a function of PEO content can be attributed to the intricate interplay of molecular interactions and electronic structure modifications within the composite material. As PEO is introduced and its content is increased, it can affect the spatial arrangement of PEDOT and PSS chains, leading to alterations in their conjugation lengths and electronic interactions. The introduction of PEO, especially at low contents, might lead to an enhanced separation between PEDOT chains, resulting in a slight increase in the band gap as observed in the transition from 0 % to 17 % PEO content. However, as the PEO content continues to increase, an increased polymer matrix disorder and potential disruption of π-conjugation in the PEDOT chains can lead to a more pronounced reduction in the band gap, as evidenced by the values at 38 % and 52 % PEO content. Interestingly, the resurgence in the band gap at 59 % PEO suggests a potential reorganization or stabilization of the PEDOT chains, possibly due to an optimal interaction or encapsulation by PEO. Additionally, PEO has been incorporated into the crystalline matrix of PEDOT:PSS to ascertain its impact on the material's electronic characteristics and to facilitate a comparison with its polymeric form. Fig. S3 shows the corresponding structures of PEDOT:PSS with 19 % PEO (Fig. S3a) and PEDOT:PSS with 38 % PEO (Fig. S3b). As could be expected, the addition of PEO enhances electronic conductivity of the crystalline structure of PEDOT:PSS. Comparing these results with the corresponding polymer based PDEOT:PSS-PEO (Fig. 5 b, c), we can conclude that the increase of PEO content

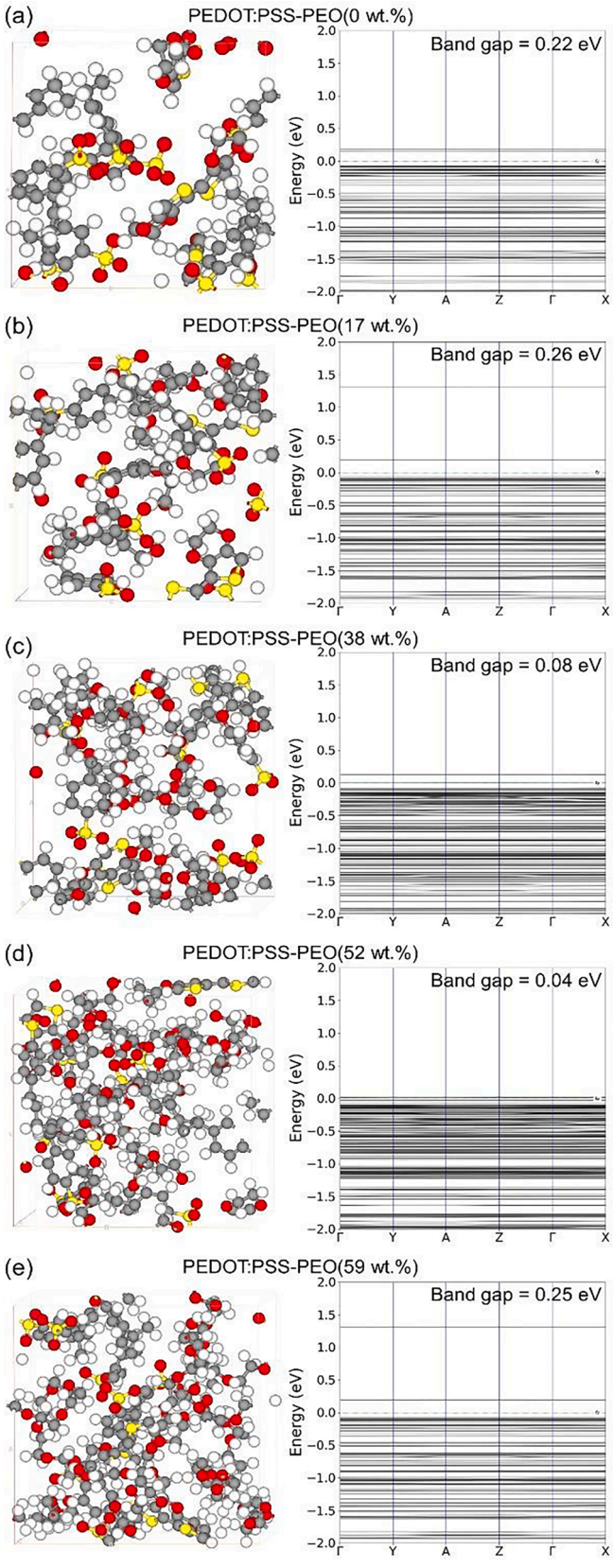

Fig. 5. Atomic structures and DFT-calculated band structures of polymeric PEDOT:PSS blends with varying PEO content. Grey spheres depict carbon atoms, red spheres are the oxygen atoms, yellow spheres are sulfur atoms, and white spheres denote hydrogen atoms. (For interpretation of the references to colour in this figure legend, the reader is referred to the web version of this article.)

enhances electronic conductivity.

The evaluation of mechanical properties using the DFT calculations revealed that Young's modulus of PEDOT:PSS without the PEO (Fig. 5a) is 478.15 MPa, followed by 597.38 MPa for 17 % PEO addition, 763.39 MPa for 38 % PEO, 765.93 MPa for 52 % and 769.37 MPa for 59 % PEO content. The Young's modulus for PEDOT:PSS without the PEO is in good agreement with the literature-reported value of 500 MPa [30]. Tan et al. [30] have performed tensile strain test experiments, where samples were standard rectangular test pieces, and the tests were conducted in a controlled environment at 25 °C with a relative humidity of 40–45 %. These tests involved stretching the samples at a tensile speed of 50 mm/min to various strain percentages, and the data were collected from multiple tests of the same sample to ensure statistical relevance. The variation in Young's modulus with differing PEO concentrations is indicative of the material's altered intermolecular interactions and structural compactness. The increment in modulus with higher PEO content suggests enhanced rigidity and potentially augmented interchain forces within the polymer blend. The relatively marginal increase in Young's modulus following a 38 % PEO concentration may be attributed to a saturation point in the PEDOT:PSS-PEO blend's capacity to accommodate additional PEO without significant alteration in mechanical reinforcement. This phenomenon can be explained by the concept of diminishing returns in the composite matrix where, beyond a certain threshold of filler content – in this case, PEO – the matrix's ability to effectively translate the addition of filler into mechanical strength enhancement is reduced.

From an application standpoint, the variable band gap offers both opportunities and challenges. A reduced band gap, as revealed at the higher PEO contents, positions the material for enhanced absorption in the near-infrared range, potentially benefiting applications like infrared photodetectors, rechargeable batteries or specialized solar cells. Conversely, the wider band gap at the lower PEO contents is more aligned with the visible spectrum, suggesting suitability for organic light-emitting diodes or specific organic photovoltaic cells. Nevertheless, while tailoring the band gap via PEO content manipulation provides versatility, it also brings forth potential drawbacks. The introduction of PEO can influence the mechanical and thermal properties of the composite, which might compromise its structural integrity or longevity in certain environments. Moreover, variations in PEO content could cause challenges related to reproducibility and consistency of electronic properties, potentially impacting device-to-device performance uniformity. In brief, while the strategic integration of PEO into PEDOT:PSS composites offers a promising avenue to engineer their electronic properties, it is imperative to holistically evaluate a specific material's characteristics to ensure its aptness for targeted optoelectronic applications.

Fig. 6 presents atomic structures and the DFT-calculated band structures of polymer PEDOT:PSS with varying PEO content at a PEDOT:PSS ratio of 0.32 corresponding to the PEDOT:PSS ratio of crystalline structure depicted in Fig. 3b. The same as with the previous results depicted in Fig. 5, Fig. 6 is organized into five vertically oriented panels, sequentially labeled from (a) to (e). Each panel is split: the left segment delineates the atomic structure of polymer PEDOT:PSS, reflecting varying PEO content levels, while the right segment offers the corresponding DFT-calculated band structure, emphasizing the resultant band gap variations due to PEO integration. Panel (a) presents PEDOT:PSS without PEO incorporation, revealing a band gap of 0.08 eV. Transitioning to panel (b), the integration of 17 % PEO yields a band gap value of 0.15 eV. Notably, in panel (c), corresponding to 38 % PEO, the band structure indicates a conductor-like behavior, marked by the absence of a discernible band gap. A subsequent increase in the PEO content to 52 %, corresponding to panel (d), results in a band gap of 0.28 eV. Strikingly, panel (e) reveals a dramatic band gap surge to 1.09 eV, commensurate with the PEO content of 59 %.

This dataset dramatically contrasts the observations from Fig. 5, where the PEDOT:PSS ratio was 2.5, as experimentally reported. The

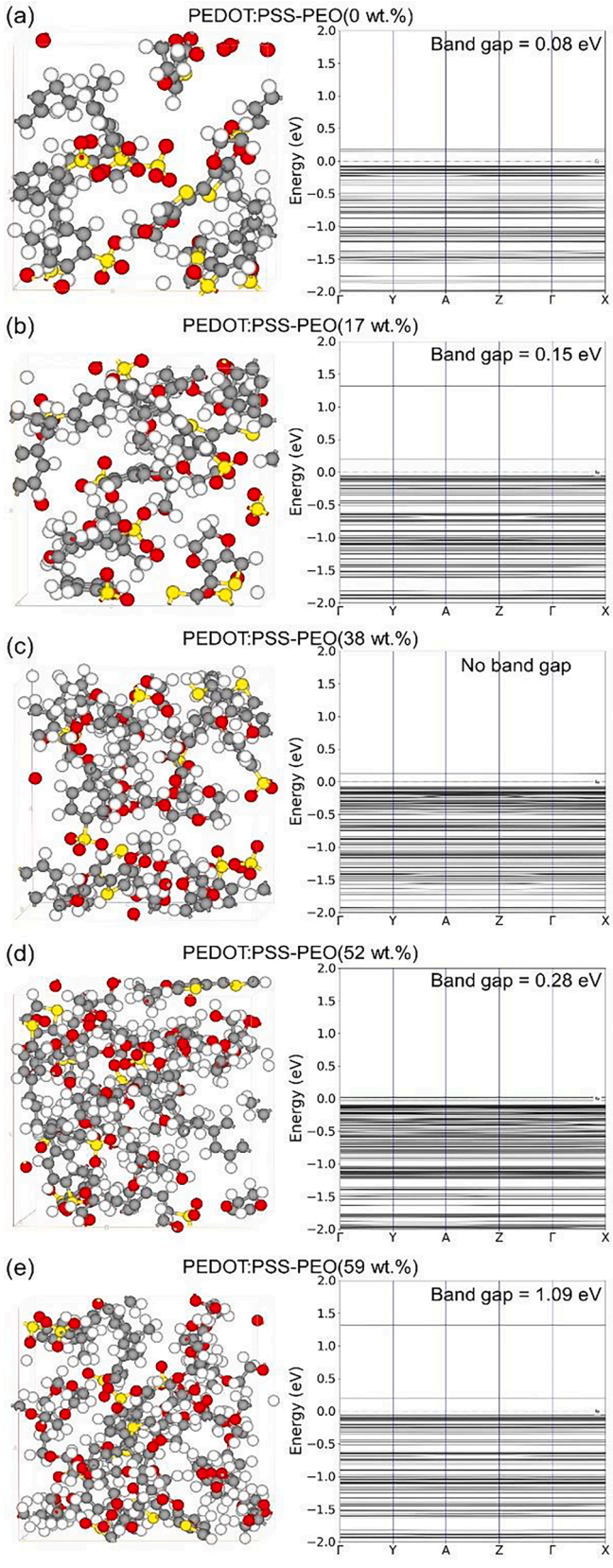

Fig. 6. Atomic structures and DFT-calculated band structures of polymer PEDOT:PSS in blends with different PEO content at a PEDOT:PSS ratio of 0.32. Grey spheres depict carbon atoms, green spheres – fluorine atoms, red spheres – the oxygen atoms, and white spheres denote hydrogen atoms. (For interpretation of the references to colour in this figure legend, the reader is referred to the web version of this article.)

pronounced difference in the PEDOT:PSS ratio, changing from 2.5 for Fig. 5 to 0.32 for Fig. 6, profoundly impacts the composite's electronic properties. The lower PEDOT:PSS ratio corresponding to Fig. 6 would require a greater PEDOT content, which, in conjunction with PEO, yields a more intricate modulation of the PEDOT electronic environment. This manifests in the wider band gap values observed in Fig. 6, especially the emergence of a conductor-like state at 38 % PEO and the substantial band gap at 59 % PEO.

From a broader perspective, the differences between the two figures (Fig. 5 vs Fig. 6) underscore a multifaceted interdependence between polymer ratios, additive content, and the resulting electronic properties. While both PEDOT:PSS ratios offer avenues to modulate band gaps by means of PEO content, the PEDOT:PSS ratio of 0.32 presents a more pronounced and dynamic range of electronic behavior. This insight is paramount for researchers and engineers aiming to tailor PEDOT:PSS blends for niche applications, balancing the intrinsic properties of such polymer blends with the additive's impact.

The evolution of a conductor-like state in the PEDOT:PSS polymer blend with 38 % PEO content is representative of a profound alteration in its electronic structure. The absence of a band gap suggests that the valence and conduction bands overlap, permitting electrons to move freely without requiring any additional energy to jump between these bands. This behavior is starkly different from semiconductors, where finite energy (the band gap) inevitably hinders electronic transitions. One possible explanation for the emergence of this conductor-like state might be in an increased disruption in the π-conjugation of the PEDOT chains due to the combined influence of PSS and PEO. This could lead to a scenario where localized states merge and form continuous bands, resulting in the observed conductor-like behavior. From an application standpoint, the emergence of a conductor-like state broadens the utility of such a polymer blend. This material could potentially serve as conductive pathways in electronic circuits or as electrodes in electronic devices, given its ability to readily transport electrons. Accordingly, this could be especially advantageous in applications where both high electrical conductivity and the inherent benefits of polymers, like flexibility and lightweight, are sought. For instance, such a structure could be used as an interfacial layer in Li metal batteries to prevent Li dendrites formation, while still allowing Li ions to pass for electrodeposition. While the conductor-like behavior augments the electrical conductivity, it could be detrimental in applications where a distinct band gap is essential, such as for photon absorption and charge separation. A conductor-like state would be unsuitable there, as it would inhibit the device's primary function of light absorption and conversion to electricity.

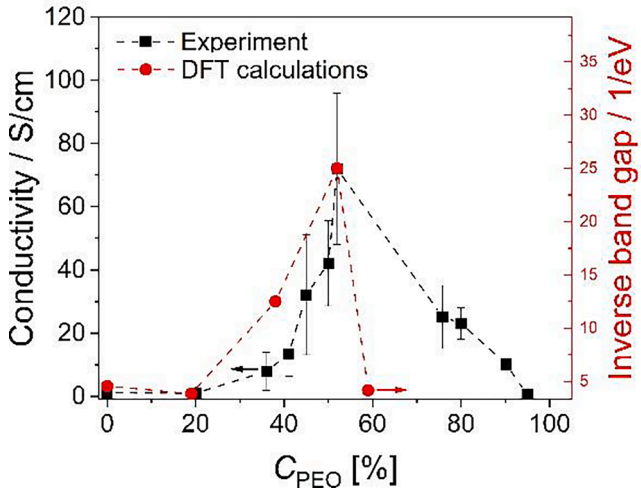

Fig. 7. Comparison of the experimentally measured electrical conductivity (left y axis) and the inverse band gap obtained from the DFT calculations (right y axis) for PEDOT:PSS with different PEO content.

Fig. 7 illustrates a comparative analysis of the experimentally measured electrical conductivity and the DFT-calculated band gaps for polymer PEDOT:PSS blends with different PEO contents. This figure contains two pivotal parameters: the experimentally measured electrical conductivity (cf. Fig. 1) and the computed inverse band gap values derived from the present DFT calculations are presented in Fig. 5. The vertical axis on the left expresses the conductivity values, while on the right – the inverse of the band gap. The horizontal axis expresses PEO content in the PEDOT:PSS blend. A salient observation from this comparative visualization is a potential correlation between the experimentally determined electrical conductivity and the computed inverse band gap. While the direct derivation of the electrical conductivity from DFT calculations poses significant challenges due to the intrinsic limitations of DFT in capturing electron–electron scattering and other many-body effects, the inverse band gap serves as a plausible proxy. A diminishing band gap, or equivalently an increasing inverse band gap, typically corresponds to a heightened electronic states' availability for conduction, possibly corroborating the observed rise in the experimental measured electrical conductivity.

The congruence between our experimentally measured conductivity (cf. Fig. 1) trend and the DFT-derived inverse band gap illustrated in Fig. 7 ascertains the merit of such indirect comparisons. The observed correlation not only underscores the relevance of band gap modifications in affecting the electronic transport properties but also provides a computational avenue to elucidate types of material behavior that might be experimentally inaccessible or challenging to measure. In brief, Fig. 7 offers a compelling narrative of the interplay between experimentally measured electrical conductivity and computed electronic properties of PEDOT:PSS blends with different PEO content. Such insights bridge the gap between theoretical predictions and empirical observations, paving the way for more focused material design and optimization of organic electronics.

Discussion on the mechanism of electronic conductivity in polymer blends. PEDOT:PSS is a composite material comprising a conductive polymer (PEDOT) and a polyelectrolyte matrix (PSS). The electronic conductivity exhibited by this blend attracted significant attention, primarily due to its relevance in organic electronics. Several theories and underlying mechanisms have been proposed to explain this conductivity. [15,17,20,31,32].

In the context of the bipolaron transport theory, the conductive state of PEDOT chains is characterized by the presence of bipolarons, resulting from oxidation processes. These entities serve as the primary charge carriers, and the resultant electrical conductivity is attributed to the movement of these bipolarons along the polymer backbone.

The percolation theory implies that within the PEDOT:PSS matrix, regions enriched with PEDOT create a percolating network, enabling efficient charge carrier transport. On the contrary, the PSS component, while behaving primarily as an insulator, enhances the blend's processability and film-forming characteristics.

Microscopically, the phase separation paradigm suggests that PEDOT:PSS films manifest distinct domains of PEDOT and PSS. This inherent phase separation facilitates the formation of conductive pathways, predominantly in the PEDOT-dominant regions, interspersed within the insulating PSS matrix. The extent of this phase separation profoundly impacts the material's electrical conductivity.

From the perspective of doping mechanisms, enhancing the conductivity of PEDOT:PSS can be achieved through the judicious removal of certain fractions of PSS, a phenomenon termed dedoping. Furthermore, introducing external dopants can increase the charge carrier density within the PEDOT chains, thereby amplifying conductivity.

The theory of morphological ordering underscores the significance of the spatial arrangement and orientation of PEDOT chains. Treatments that foster chain alignment or crystallinity are likely to bolster charge transport. Various post-treatment modalities, including solvent annealing or thermal protocols, have the potential to alter the morphological

landscape of PEDOT:PSS films, affecting their conductive properties.

The hydration-effect theory elucidates the role of water molecules in modulating the PEDOT:PSS conductivity. While water can promote reconfiguration of PSS chains, optimizing charge transport pathways, an overabundance of hydration or ambient humidity may instigate material degradation or conductivity attenuation. Alternatively, Wang et al. [4] have shown that the high-humidity post-treatment increases PEDOT:PSS conductivity.

Lastly, the notion of secondary doping involves the integration of supplementary dopants or additives to augment the conductivity of PEDOT:PSS, either by introducing additional charge carriers or through morphological modifications.

It should be emphasized that the above-mentioned phenomena are not isolated but can operate synergistically. The manifestation of specific electronic properties in PEDOT:PSS and its blends are contingent upon its synthesis, formulation, and external conditions.

The electronic structure of PEDOT is dominated by polarons and bipolarons, which arise due to the doping process. Polarons are a singly charged species, whereas bipolarons are doubly-charged. The understanding of polaron and bipolaron formation provides an insight into the electronic and optical properties of PEDOT. The presence of these charged species explains the high electrical conductivity of doped PEDOT. Polarons and bipolarons are highly mobile charge carriers, which makes PEDOT suitable for various electronic applications. The possible limitations stem from the fact that polaron and bipolaron concentrations can be affected by the doping level, temperature, and other external factors, making it crucial to maintain controlled conditions for consistent electronic properties. Zozoulenko et al. [17] reported DFT calculations of band structure of PEDOT. They discuss the formation of the polaronic band, which lies between the valence and conduction bands. When PEDOT is doped, new electronic states emerge, leading to the appearance of the polaronic and bipolaronic bands. It was revealed that the position and width of a polaronic band can be tuned by varying the doping level, offering flexibility in designing PEDOT-based devices. However, the exact position of the polaronic and bipolaronic bands can vary depending on the computational method used, potentially leading to discrepancies between the experimental and theoretical results. Zozoulenko et al. also discuss the role of counterions, and, especially, the role of counterions in stabilizing polarons and bipolarons. The choice of a counterion can influence the spatial distribution and mobility of these charged species. Selecting appropriate counterions is beneficial because one can tailor the electronic properties of PEDOT for specific applications. Counterions can also play a role in enhancing the structural stability of PEDOT films. A limitation could stem from the interaction between counterions and polarons/bipolarons, which can be complex and may vary with the nature of the counterion, requiring detailed studies for each system. Zozoulenko et al. also provide insights into the optical properties of PEDOT by analyzing its absorption spectra. The presence of polarons and bipolarons leads to characteristic absorption peaks. Optical absorption spectra serve as a non-destructive tool to probe the concentration and distribution of polarons and bipolarons in PEDOT. The spectra provide information about electronic transitions, aiding in the design of optoelectronic devices. However, the interpretation of the spectra can be complex due to overlapping peaks and the influence of various factors, such as film thickness and doping level.

Upon evaluating our present combined DFT and experimental results to elucidate the electronic behavior of PEDOT:PSS-PEO composites, the data inclines towards the manifestation of polaronic rather than bipolaronic conductivity. It should be emphasized that these observations are based on indirect evidence and preliminary data. This assertion is substantiated by the charge density differential analysis depicted in Fig. S4, wherein the isosurface of 0.65 eV/Å^{-3} corresponds to the covalent radius of an oxygen atom, showing no supplementary density that would suggest bipolaronic activity. This observation intimates a polaron-driven conducting mechanism within the blend. Furthermore, when considering the intricate geometrical configurations of these composites, it is plausible to postulate that the percolation theory may contribute to the elucidation of the conductive pathways. The interplay of the polaronic mechanism, characterized by the localized distortion of the polymer chain accommodating a charge carrier, and the percolation theory, which describes the critical concentration threshold for establishing a conducting network, collectively facilitates a comprehensive understanding of the electrical conductivity phenomena within PEDOT:PSS-PEO blends. Such a dualistic approach enables a more nuanced interpretation of the electronic transport properties in these sophisticated materials.

4. Summary and conclusions

The present study explores PEDOT:PSS-PEO polymer blends with different PEDOT, PSS, and PEO content, leading to the discovery of unexpected electronic properties in these polymer blends. Remarkably, the introduction of PEO induces a profound impact on the band gap, particularly near the 52 wt% PEO content. Additionally, the PEDOT to PSS ratio plays a crucial role in determining the band gap. The DFT-calculated electronic properties of PEDOT:PSS with the same ratio as for the crystalline PEDOT:PSS structure revealed the emergence of a conductor-like state at a 38 wt% PEO concentration. These findings reveal the sensitivity of the polymer's electronic behavior to both the ratio of PEDOT:PSS and the content of PEO additive, demonstrating the potential for precise electronic property tailoring in applications ranging from conductive pathways to electrode materials in energy storage devices. In addition, our research revealed that the electronic conductivity in PEDOT:PSS-PEO composites is predominantly polaronic, as evidenced by the charge density differentials and the absent bipolaronic signatures, with the conductivity phenomena further explicated by the synergy between localized polaronic distortions and the macroscopic principles of percolation theory. That offers a dualistic framework for understanding complex electronic transport behavior in these advanced polymeric systems. Overall, the present theoretical findings are in excellent agreement with the independent measurements of the electrical conductivity, which was measured in the present work using films of PEDOT:PSS-PEO.

In addition, the DFT-based mechanical property evaluation of PEDOT:PSS-PEO blends has corroborated experimental findings, describing an increase in Young's modulus (a stiffening) with an incremental increase in PEO content, with a noted plateau beyond 38 % PEO indicative of a saturation point in mechanical reinforcement. This study underscores the critical interplay between filler content and composite matrix behavior, emphasizing the necessity for optimization of PEO concentration to achieve desired material properties for targeted applications.

This combined modeling and experimental approach provides a physical interpretation of the underlying factors responsible for the observed variations in the electrical conductivity in PEDOT:PSS-PEO systems. These insights pave the way for the development of highly conducting polymer blends suitable for extrusion-based manufacturing techniques such as DIW, thus contributing to the advancement of e-textile technologies and other electronic applications.

CRediT authorship contribution statement

Vitaliy Yurkiv: Conceptualization, Formal analysis, Funding acquisition, Investigation, Methodology, Project administration, Writing – original draft, Writing – review & editing. **Xinnian Wang:** Investigation, Writing – original draft, Writing – review & editing. **Yongil Kim:** Formal analysis, Investigation, Writing – original draft, Writing – review & editing. **Yayue Pan:** Formal analysis, Funding acquisition, Project administration, Writing – original draft, Writing – review & editing. **Farzad Mashayek:** Formal analysis, Funding acquisition, Project administration, Writing – original draft, Writing – review & editing.

Alexander L. Yarin: Conceptualization, Formal analysis, Funding acquisition, Investigation, Methodology, Project administration, Writing – original draft, Writing – review & editing.

Declaration of competing interest

The authors declare that they have no known competing financial interests or personal relationships that could have appeared to influence the work reported in this paper.

Data availability

Data will be made available on request.

Acknowledgements

The authors acknowledge the financial support from the National Science Foundation awards CBET 2312197 and 2224749. DFT calculations were performed using the High-Performance Computing (HPC) resources supported by the University of Arizona TRIF, UITS, and Research, Innovation, and Impact (RII) and maintained by the UArizona Research Technologies department. In addition, this work partially used SDSC Dell Cluster with AMD Rome HDR IB (Expanse) allocation TRA220030. VY would like to acknowledge Sara M. Willis for HPC cluster support.

Appendix A. Supplementary data

Supplementary data to this article can be found online at https://doi.org/10.1016/j.jcis.2024.06.148.

References

[1] M.N. Gueye, A Carella, J. Faure-Vincent, R. Demadrille, J.P. Simonato, Progress in understanding structure and transport properties of PEDOT-based materials: a critical review, Prog. Mater. Sci. Elsevier Ltd February 1, 2020. doi: 10.1016/j.pmatsci.2019.100616.
[2] H. Shi, C. Liu, Q. Jiang, J. Xu, Effective approaches to improve the electrical conductivity of PEDOT:PSS: a review, Adv. Electron. Mater. 1 (4) (2015), https://doi.org/10.1002/aelm.201500017.
[3] C. Yi, A. Wilhite, L. Zhang, R. Hu, S.S.C. Chuang, J. Zheng, X. Gong, Enhanced thermoelectric properties of poly(3,4-ethylenedioxythiophene):poly (styrenesulfonate) by binary secondary dopants, ACS Appl. Mater. Interf. 7 (17) (2015) 8984–8989, https://doi.org/10.1021/acsami.5b01960.
[4] X. Wang, J. Plog, K.M. Lichade, A.L. Yarin, Y. Pan, Three-dimensional printing of highly conducting PEDOT: PSS-based polymers, J. Manuf. Sci. Eng. 145 (1) (2023), https://doi.org/10.1115/1.4055850.
[5] Z. Fan, J. Ouyang, Thermoelectric properties of PEDOT:PSS, in: *Advanced Electronic Materials*, Blackwell Publishing Ltd, 2019., https://doi.org/10.1002/aelm.201800769.
[6] J.H. Lee, Y.R. Jeong, G. Lee, S.W. Jin, Y.H. Lee, S.Y. Hong, H. Park, J.W. Kim, S. S. Lee, J.S. Ha, Highly conductive, stretchable, and transparent PEDOT:PSS electrodes fabricated with triblock copolymer additives and acid treatment, ACS Appl. Mater. Interf. 10 (33) (2018) 28027–28035, https://doi.org/10.1021/acsami.8b07287.
[7] A.V. Kubarkov, O.A. Drozhzhin, E.A. Karpushkin, K.J. Stevenson, E.V. Antipov, V. G. Sergeyev, Poly(3,4-ethylenedioxythiophene):poly(styrenesulfonic acid)–polymer composites as functional cathode binders for high power LiFePO 4 batteries, Colloid Polym. Sci. 297 (3) (2019) 475–484, https://doi.org/10.1007/s00396-018-04468-0.
[8] N.A. Shahrim, Z. Ahmad, A. Wong Azman, Y. Fachmi Buys, N. Sarifuddin, Mechanisms for doped PEDOT:PSS electrical conductivity improvement, in: Materials Advances, Royal Society of Chemistry, 2021, pp. 7118–7138, https://doi.org/10.1039/d1ma00290b.
[9] J. Plog, X. Wang, K.M. Lichade, Y. Pan, A.L. Yarin, Extremely-fast electrostatically-assisted direct ink writing of 2D, 2.5D and 3D functional traces of conducting polymer poly(3,4-ethylenedioxythiophene) polystyrene sulfonate- polyethylene oxide (PEDOT:PSS-PEO), J. Colloid Interface Sci. 651 (2023) 1043–1053, https://doi.org/10.1016/j.jcis.2023.07.206.
[10] D.H. Yoon, S.H. Yoon, K.S. Ryu, Y.J. Park, PEDOT:PSS as multi-functional composite material for enhanced li-air-battery air electrodes, Sci. Rep. (2016) 6, https://doi.org/10.1038/srep19962.
[11] X. Ye, C. Wang, L. Wang, B. Lu, F. Gao, D. Shao, DLP Printing of a flexible micropattern Si/PEDOT:PSS/PEG electrode for lithium-ion batteries, Chem. Commun. (2022), https://doi.org/10.1039/d2cc01626e.
[12] M.R. Shaik, M.J. Yeo, K.Y. Cho, S. Yoon, Robust artificial HfO2/PEDOT:PSS polarity layer for increasing stability of Li metal anodes, J Alloys Compd (2023,) 939, https://doi.org/10.1016/j.jallcom.2023.168703.
[13] K. Fu, R. Lv, B. Na, S. Zou, R. Zeng, B. Wang, H. Liu, Mixed ion-electron conducting PEO/PEDOT: PSS miscible blends with intense electrochromic response, Polymer (Guildf) (2019) 184, https://doi.org/10.1016/j.polymer.2019.121900.
[14] E.G. Kim, J.L. Brédas, Electronic evolution of Poly(3,4-ethylenedioxythiophene) (PEDOT): from the isolated chain to the pristine and heavily doped crystals, J. Am. Chem. Soc. 130 (50) (2008) 16880–16889, https://doi.org/10.1021/ja806389b.
[15] A. Lenz, H. Kariis, A. Pohl, P. Persson, L. Ojamäe, The electronic structure and reflectivity of PEDOT:pss from density functional theory, Chem. Phys. 384 (1–3) (2011) 44–51, https://doi.org/10.1016/j.chemphys.2011.05.003.
[16] B. Zhang, K. Wang, D. Li, X. Cui, Doping effects on the thermoelectric properties of pristine poly(3,4-ethylenedioxythiophene), RSC Adv. 5 (43) (2015) 33885–33891, https://doi.org/10.1039/c4ra16451b.
[17] I. Zozoulenko, A. Singh, S.K. Singh, V. Gueskine, X. Crispin, M. Berggren, Polarons, bipolarons, and absorption spectroscopy of PEDOT, ACS Appl. Polym. Mater. 1 (1) (2019) 83–94, https://doi.org/10.1021/acsapm.8b00061.
[18] W. Michaels, Y. Zhao, J. Qin, Atomistic modeling of PEDOT:PSS complexes I: DFT benchmarking, Macromolecules 54 (8) (2021) 3634–3646, https://doi.org/10.1021/acs.macromol.1c00351.
[19] W. Michaels, Y. Zhao, J. Qin, Atomistic modeling of PEDOT:PSS complexes II: force field parameterization, Macromolecules 54 (12) (2021) 5354–5365, https://doi.org/10.1021/acs.macromol.1c00860.
[20] W. Shi, T. Zhao, J. Xi, D. Wang, Z. Shuai, Unravelling doping effects on PEDOT at the molecular level: from geometry to thermoelectric transport properties, J. Am. Chem. Soc. 137 (40) (2015) 12929–12938, https://doi.org/10.1021/jacs.5b06584.
[21] R.O. Agbaoye, P.O. Adebambo, J.O. Akinlami, T.A. Afolabi, S.Z. Karazhanov, D. Ceresoli, G.A. Adebayo, Elastic constants and mechanical properties of PEDOT from first principles calculations, Comput. Mater. Sci. 139 (2017) 234–242, https://doi.org/10.1016/j.commatsci.2017.07.042.
[22] K. Burke, Perspective on density functional theory, J. Chem. Phys. (2012) 136 (15), https://doi.org/10.1063/1.4704546.
[23] G. Kresse, From ultrasoft pseudopotentials to the projector augmented-wave method, Phys. Rev. B 59 (3) (1999) 1758–1775, https://doi.org/10.1103/PhysRevB.59.1758.
[24] G. Kresse, J. Furthmüller, Efficient iterative schemes for ab initio total-energy calculations using a plane-wave basis set, Phys. Rev. B Condens Matter Mater. Phys. 54 (16) (1996) 11169–11186, https://doi.org/10.1103/PhysRevB.54.11169.
[25] G. Kresse, J. Hafner, Ab initio molecular dynamics for liquid metals, Phys. Rev. B 47 (1) (1993) 558–561, https://doi.org/10.1103/PhysRevB.47.558.
[26] S. Grimme, Semiempirical GGA-type density functional constructed with a long-range dispersion correction, J. Comput. Chem. 27 (15) (2006) 1787–1799, https://doi.org/10.1002/jcc.20495.
[27] J. Balaji, K. Aruchamy, T.H. Oh, Binder-free PEO/PPy/PEDOT:PSS layer coated on nickel foam for high-performance asymmetric supercapacitor applications, Ionics (kiel) 28 (10) (2022) 4867–4880, https://doi.org/10.1007/s11581-022-04692-3.
[28] Bernard Dennis Cullity, Elements of X-Ray Diffraction, Addison-Wesley, 1956.
[29] D. Farka, K. Kříž, J. Fanfrlík, Strategies for the design of PEDOT analogues unraveled: the use of chalcogen bonds and σ-holes, J. Phys. Chem. A 127 (17) (2023) 3779–3787, https://doi.org/10.1021/acs.jpca.2c08965.
[30] P. Tan, H. Wang, F. Xiao, X. Lu, W. Shang, X. Deng, H. Song, Z. Xu, J. Cao, T. Gan, B. Wang, Z.X. Solution-Processable, Soft, self-adhesive, and conductive polymer composites for soft electronics, Nat. Commun. 13 (1) (2022), https://doi.org/10.1038/s41467-022-28027-y.
[31] S. Nešpůrek, P. Kuberský, R. Polanský, M. Trchová, J. Šebera, V. Sychrovský, Raman spectroscopy and DFT calculations of PEDOT:PSS in a dipolar field, Phys. Chem. Chem. Phys. 24 (1) (2022) 541–550, https://doi.org/10.1039/d1cp03899k.
[32] J. Alam, X. Xu, P.C.O. Adu, Q. Meng, K. Zuber, S. Afshar, H.-C. Kuan, J. Ma, Enhancing thermoelectric performance of PEDOT: PSS: a review of treatment and nanocomposite strategies, Adv. Nanocompos. (2023), https://doi.org/10.1016/j.adna.2023.08.001.